ACS Macro Letters

Letter

pubs.acs.org/macroletters

Tri-Phasic Size- and Janus Balance-Tunable Colloidal Nanoparticles (JNPs)

Chunliang Lu and Marek W. Urban*

Department of Materials Science and Engineering and Center for Optical Materials and Engineering Technologies (COMSET), Clemson University, Clemson, South Carolina 29634-0915, United States

Supporting Information

ABSTRACT: These studies show synthesis of triphasic size- and Janus balance (JB)-tunable nanoparticles (JNPs) utilizing a two-step emulsion polymerization of pentafluorostyrene (PFS) and 2-(dimethylamino)ethyl methacrylate (DMAEMA) and *n*-butyl acrylate (nBA) in the presence of poly(methyl methacrylate (MMA)/nBA) nanoparticle seeds. Each JNP consists of three phase-separated copolymers: p(MMA/nBA) core, temperature, and pH-responsive (p(DMAEMA/nBA)) phase capable of reversible size and shape changes, and shape-adoptable (p(PFS/nBA)) phase. Due to built-in second-order lower critical solution temperature (II-LCST) transition of p-(DMAEMA/nBA) copolymer, macromolecular segments collapse when temperature increases from 30 to 45 °C, resulting in size and shape changes. The p(DMAEMA/nBA) and p(MMA/nBA) phases within each JNP assume concave, flat, or convex shapes, forcing p(PFS/nBA) phase to adopt convex, planar, or concave interfacial curvatures, respectively. As a result, the JB can be tuned from 3.78 to 0.72. The presence of pH-responsive DMAEMA component also facilitates the size and JB changes due to protonation of the tertiary amine groups of p(DMAEMA/nBA) backbone. Synthesized in this manner, JNPs are capable of stabilizing oil droplets in water at high pH to form Pickering emulsions, which at lower pH values release oil phase. This process is reversible and can be repeated many times.

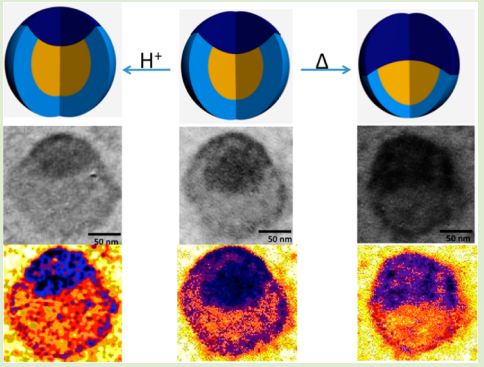

While imparting distinctly different physical and chemical properties into single colloid, Janus particles (JPs) have attracted widespread attention because of its numerous technological advantages.[1−4] Various approaches have been utilized in their synthesis, including microfluidics,[1,5,6] block copolymer assembly,[7−9] masking technique,[10−13] heterogeneous nucleation,[14,15] flame synthesis,[16] and emulsion polymerization.[17−19] Of particular scientific interest, and perhaps most challenging, is the synthesis of large quantities of Janus nanoparticles (JNPs) with precisely defined morphologies capable of responding to a variety of external or internal stimuli.[20,21] The presence of stimuli-responsiveness built into JNPs may be beneficial in a variety of applications, particularly, if the particles are able to self-assemble in complex hierarchical morphologies.[8,22,23] Building on controllable synthesis of "acorn-shape" JNPs using seeded emulsion polymerization,[17] shape evolution control of JNPs was achieved by adjusting the glass transition temperature (T_g) via compositional gradients during copolymerization.[18] Furthermore, incorporating photochromic entities into shape-adjustable JNPs also facilitated tunable color changes.[19] One of the intriguing properties of JPs is their enhanced interfacial activities[24] and Janus balance (JB), defined as the ratio of hydrophilic and hydrophobic components,[25] is introduced to quantify the geometry of the JPs as well as their interfacial activities. However, only a few studies have demonstrated procedures capable of controlling JB values of JPs during the synthesis process, such as controlling the flow rate of monomers in microfluidic synthesis of JPs,[5] controlling the exposed area of particles to be chemically modified,[25−28] or controlling of the block lengths of block terpolymers that self-assemble into JNPs.[29] However, introducing stimuli-responsive components into JNPs with the capable of tuning JB values will offer numerous advantages. In these studies we focused on the synthesis of triphasic shape-tunable JNPs, where p(DMAEMA/nBA) phase within each nanoparticle is capable of reversible shape tunability induced by temperature and/or pH changes, while p(MMA/nBA) and p(PFS/nBA) phases remain passive, yet capable of adapting to shape changes of the adjacent phases. Finally, we demonstrate the interfacial activities of JNPs by stabilizing oil droplets in water at different pH values.

Figure 1A illustrates a two-step synthesis of stimuli-responsive JNPs from p(MMA/nBA) colloidal seed particles. During the first step, PFS and nBA were copolymerized under monomer-starvation conditions in the presence of previously synthesized spherical p(MMA/nBA) seed emulsions with an average particle size of 86 nm (Figure 1B-a). Due to substantial interfacial energy differences between fluorinated and acrylate phases, this process favors the formation of phase-separated

Received: January 15, 2014
Accepted: March 13, 2014
Published: March 25, 2014

   dx.doi.org/10.1021/mz500029z | *ACS Macro Lett.* 2014, 3, 346−352

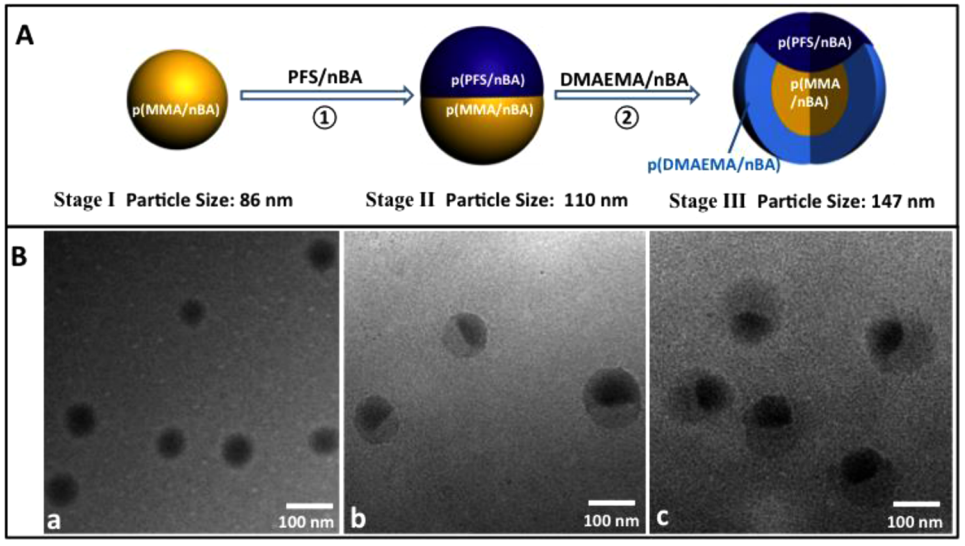

Figure 1. (A) Schematic diagram of the synthetic process of stimuli-responsive JNPs. (B) TEM images of p(MMA/nBA) (B-a), p(MMA/nBA)-p(PFS/nBA) (B-b), and p(MMA/nBA)-p(PFS/nBA)-p(DMAEMA/nBA) nanoparticles (B-c).

JNPs with an average particle size of 110 nm shown in TEM images of Figure 1B-b. Compared with the p(MMA/nBA) phase, p(PFS/nBA) phase in the JNPs appears darker due to higher electron density of fluorine components. The second step involved copolymerization of temperature and/or pH responsive DMAEMA along with nBA monomers on the top of phase-separated p(MMA/nBA)-p(PFS/nBA) JNPs, giving a three phase system: p(MMA/nBA)-p(PFS/nBA)-p-(DMAEMA/nBA). Figure 1B-c illustrates the final product which exhibits an average particle size of 147 nm. The choice of p(DMAEMA/nBA) was dictated by temperature and pH responsiveness, whereas p(MMA/nBA) and p(PFS/nBA) copolymers are able to form phase-separated JNP cores.

It is well established that during semicontinuous emulsion polymerization under monomer-starvation conditions monomers and growing oligomeric radicals continuously diffuse into existing particles instead of forming new particles. As a result, the particle size increases. As noted in the earlier studies,[18] the shape of the resulting particles is dictated by the ability of individual phases to minimize total interfacial energy during polymerization. To correlate synthetic efforts responsible for morphological features shown in TEM images in Figure 1, let us consider the surface energy differences within this tertiary copolymer system. To determine surface energy values of the individual copolymer phases, surfactant-free colloidal particles of the same composition were synthesized. Upon being centrifuged, dried, dissolved in toluene, and spin-coated, p(MMA/nBA), p(PFS/nBA), and p(DMAEMA/nBA) films were produced. While the results of static contact angle measurements using water and hexadecane are summarized in Table 1, Supporting Information (sections 1 and 2), provide further details regarding determination of surface energies.

As shown in Table 1A, surface energies of p(MMA/nBA), p(PFS/nBA), and p(DMAEMA/nBA) are 38.5, 23.0, and 39.4 mN/m, respectively. It is quite apparent that p(PFS/nBA) exhibits significantly smaller surface energy values compared to p(MMA/nBA) and p(DMAEMA/nBA). The surface energies for each copolymer as well as polar and dispersive contributions shown in Table 1A allow us to estimate the interfacial surface tension between two phases in individual JNPs. The results summarized in Table 1B show that the interfacial surface

Table 1. (A) Static Contact Angle Measurement Data and Surface Energy Results of the Copolymer Films; (B) Interfacial Surface Tension between p(MMA/nBA) and p(PFS/nBA), p(PFS/nBA) and p(DMAEMA/nBA), and p(MMA/nBA) and p(DMAEMA/nBA), Respectively

A

copolymers (mN/m)	static contact angle: water (°)	static contact angle: hexadecane (°)	γ^{d}_{sv} (mN/m)	γ^{p}_{sv} (mN/m)	γ
p(MMA/nBA)	71.2	0	27.5	11.0	38.5
p(PFS/nBA)	97.0	42.3	20.8	2.2	23.0
p(DMAEMA/nBA)	69.5	0	27.5	11.9	39.4

B

copolymers	interfacial surface tension γ_{12}
p(MMA/nBA)-p(PFS/nBA)	6.80
p(DMAEMA/nBA)-p(PFS/nBA)	7.43
p(MMA/nBA)-p(DMAEMA/nBA)	0.04

tension between p(MMA/nBA) and p(PFS/nBA), p-(DMAEMA/nBA) and p(PFS/nBA), and p(MMA/nBA) and p(DMEEMA/nBA) are 6.80, 7.43, and 0.04 mN/m, respectively. These data indicate that when PFS/nBA were copolymerized in the presence of p(MMA/nBA) seed (Figure 1B-a), significant interfacial surface tension (6.8 mN/m) between the two copolymers favors the minimum contact surface area within each particle, resulting in the formation of phase-separated JNPs (Figure 1B-b).[17−19] Furthermore, when DMAEMA and nBA monomers were copolymerized on the p(MMA/nBA)-p(PFS/nBA) core under monomer-starvation conditions, p(DMAEMA/nBA) also phase-separates from p(PFS/nBA) fluorinated hemisphere and resides near the least hydrophobic nonfluorinated p(MMA/nBA) copolymer phase in order to minimize the total interfacial surface energy within the triphasic JNPs. Also, instead of diffusing into p(MMA/nBA) phase and forming inverse core−shell morphologies, higher hydrophilicity of p(DMAEMA/nBA) facilitates polymerization on the surface of p(MMA/nBA) hemispherical core. As a result, stimuli-responsive JNPs shown in Figure 1B-c are produced. Although similarities of p(MMA/

dx.doi.org/10.1021/mz500029z | ACS Macro Lett. 2014, 3, 346−352

nBA) and p(DMAEMA/nBA) copolymer electron densities make the two phases of the half core−shell hemisphere not easily distinguishable by TEM, the particle size analysis shows the particle growth from 110 to 147 nm further substantiating the formation of stimuli-responsive JNPs during stage III shown in Figure 1A.

Molecular thermodynamics simulations were also employed in which three random copolymers p(MMA/nBA), p(PFS/nBA), and p(DMAEMA/nBA) containing 50 repeating units were allowed to equilibrate to reach the minimum energy state. The results of these simulations are shown in Figure 2, where

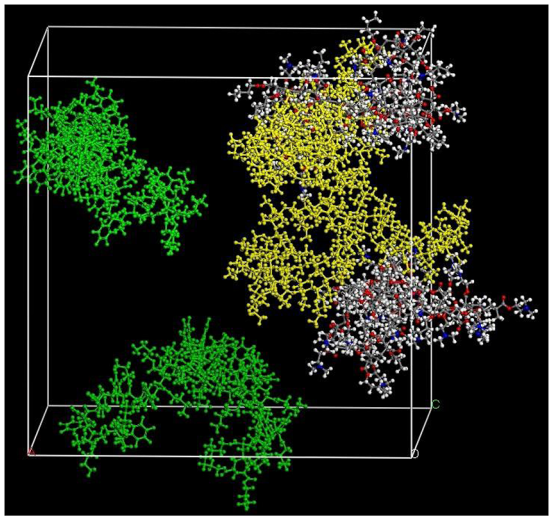

Figure 2. Computer simulations illustrating triphase copolymers in one amorphous cell: p(MMA/nBA) yellow, p(PFS/nBA) green, and p(DMAEMA/nBA) (white for H, gray for C, red for O, blue for N). As shown, phase separation between p(PFS/nBA) and p(MMA/nBA) as well as p(DMAEMA/nBA) occurs. In contrast, p(MMA/nBA) and p(DMAEMA/nBA) are compatible.

p(PFS/nBA) polymer chains (green) are apart from both p(MMA/nBA) (yellow) and p(DMAEMA/nBA) segments due to their incompatibility leading to phase-separation within one colloidal particle. In contrast, p(DMAEMA/nBA) and p(MMA/nBA) segments remain compatible manifested by the entanglements, indicating that p(DMAEMA/nBA) phase prefers to remain on the nonfluorinated p(MMA/nBA) hemisphere. Table S1 of the Supporting Information provide energy values between each copolymer after the unit cell has been equilibrated. As shown, the unfavorable equilibrium state for copolymers is manifested by highest energy values which are 9164 and 9467 kcal/mol for p(MMA/nBA)-p(PFS/nBA) and p(DMAEMA/nBA)-p(PFS/nBA), respectively. It should be pointed out that these modeling exercises do not take into account the interfacial energy considerations during polymerization, thus neglecting the role of solvent (water) and surface active components (surfactants).

To illustrate stimuli-responsiveness and the ability to form tunable shapes, p(MMA/nBA)-p(PFS/nBA)-p(DMAEMA/nBA) JNPs were exposed to pH = 8 at 25, 35, 38, 40, and 45 °C, respectively. TEM images in Figure 3a, A−E, as well as their close-ups shown in Figure 3a(A′−E′) illustrate that when temperature increases from 25 to 45 °C, the fluoropolymer shape changes from spherical to ellipsoidal. At 25 °C, the interfacial tension between p(MMA/nBA)-p(DMAEMA/nBA) and p(PFS/nBA) phases forces JNPs to form equilibrated hemispherical morphologies with a convex shape of p(PFS/nBA) phase. Upon the temperature increase to 35 °C, p(DMAEMA/nBA) phase begin approaching the second-order low critical solution temperature (II-LCST) transition, resulting in the collapsed p(DMAEMA/nBA) phase.[30] As a consequence, the temperature increase from 30 to 46 °C causes the JNPs to shrink gradually from 147 to 131 nm (Supporting Information, section 3, Figure S1). It should be noted that the three copolymers exhibit glass transition temperature (T_g) below 25 °C (Supporting Information, section 4, Figure S2), which facilitates free rotation of polymer backbones and rearrangement of polymer chains during II-LCST temperature range in order to reach equilibrated particle morphologies. The collapse of p(DMAEMA/nBA) segments also increases the magnitude of hydrophobic interactions within this phase, causing shrinkage of p(MMA/nBA) hemisphere core as well as expansion of the outer p(PFS/nBA) hemisphere layer. As a result, JNPs assume a new shape with a less convex interface of the p(PFS/nBA) phase. Because p(DMAEMA/nBA) random copolymers exhibit a II-LCST transition over a broad temperature range, as temperature increases further, p(DMAEMA/nBA) backbones continue to collapse, leading to an almost planar interface at 38 °C. At the same time, the volume of single stimuli-responsive particles decreased by ∼19%. When temperature reaches above 40 °C, a concave interface is assumed, which is further expanded at higher temperatures to reach shrinkage values as high as ∼29%. This shape-tunable behavior is a repetitive process in aqueous environments.

During this temperature induced process particle morphologies and the interfacial curvature between the two phase-separated hemispheres of the JNPs is being continuously altered, resulting in the hydrophilic-to-hydrophobic surface area ratio known as the Janus Balance (JB) tunability induced by temperature changes. Supporting Information, section 4, provide further details regarding the JB determination. As shown in Figure 3a(A″−E″), at 25 °C, the JB is 3.78 (79.1/20.9) and is dominated by hydrophilic hemisphere. However, as a result of p(DMAEMA/nBA) collapse at elevated temperatures, the relative surface area of hydrophilic hemisphere decreases while the relative area of hydrophobic hemisphere increases, leading to the decrease of the JB to 1.60 (61.6/38.4) at 38 °C. When temperature reaches 40 °C, the relative surface areas of hydrophilic and hydrophobic hemispheres become almost the same and the JB is 0.98 (49.5/50.5), which upon temperature increase to 45 °C, further decreases to 0.72 (41.7/58.3).

Due to the expansion of p(DMAEMA/nBA) phase induced by protonation of the tertiary amine functional groups in acidic environments, particle size of the JNPs increases from 145 to 163 nm as pH decreases from 10 to 4 at 25 °C (Supporting Information, Figure S2). Figure 3b illustrates the size and morphology changes of these same JNPs as a function of pH. As seen, when pH decreases from 10 to 4, the interface for p(PFS/nBA) hemisphere becomes more convex while its size remain almost unchanged whereas the nonfluorinated p(MMA/nBA)-p(DMAEMA/nBA) hemisphere size increases, which means that hydrophilic−hydrophobic hemisphere ratio increases. As a result, JB values of the JNPs increase from 3.42 (77.4/22.6) at pH = 10 to 4.24 (80.9/19.1) at pH = 6 and further increase to 4.52 (81.9/18.1) at pH = 4. These relatively small changes are likely attributed to the limited penetration of acid groups during protonation by aqueous HCl as well as the

dx.doi.org/10.1021/mz500029z | ACS Macro Lett. 2014, 3, 346−352

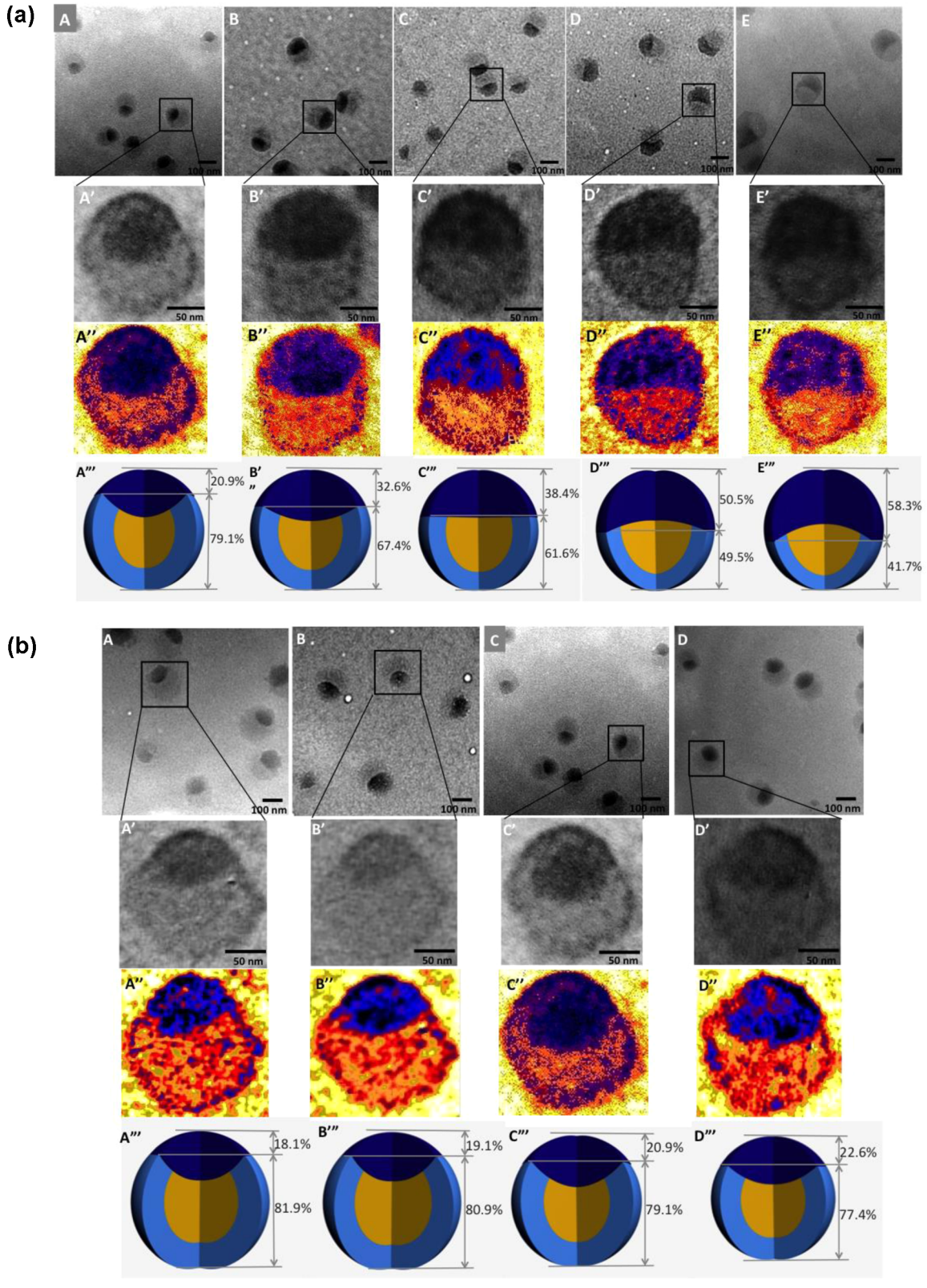

Figure 3. (a) TEM (A–E and A′–E′) images of p(MMA/nBA)-p(PFS/nBA)-p(DMAEMA/nBA) nanoparticles at 25 (A/A′), 35 (B/B′), 38 (C/C′), 40 (D/D′), and 45 (E/E′); Images A″–E″ were obtained using image analysis, as described in the Experimental Section; Dimensional changes of the JNPs at 25, 35, 38, 40, and 45 °C are schematically depicted in A‴–E‴, respectively. (b) TEM (A–D and A′–D′) images of p(MMA/nBA)-p(PFS/nBA)-p(DMAEMA/nBA) nanoparticles at pH = 4 (A/A′), 6 (B/B′), 8 (C/C′), and 10 (D/D′). Images A″–D″ were obtained using image analysis, as described in the Experimental Section; Dimensional changes of the particles at pH = 4, 6, 8, and 10 are schematically depicted in A‴–D‴, respectively.

dx.doi.org/10.1021/mz500029z | ACS Macro Lett. 2014, 3, 346–352

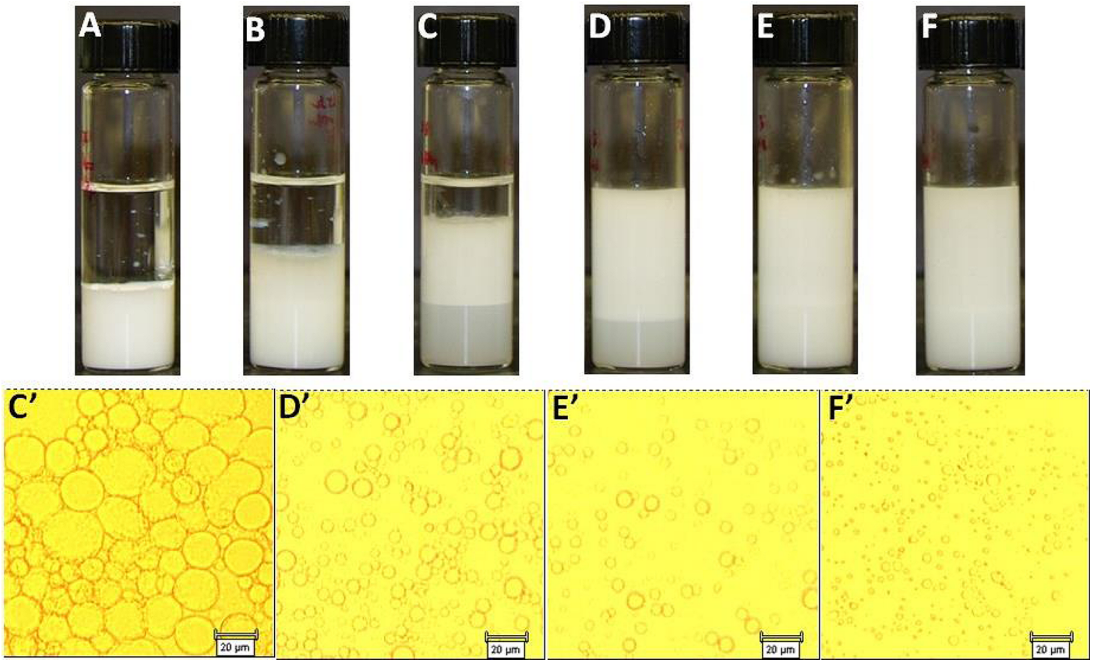

Figure 4. Photographs of dodecan/water mixture after 2000 rpm for 10 min at 25 °C in the presence of p(MMA/nBA) particles (A), p(MMA/nBA)-p(PFS/nBA) particles (B), p(MMA/nBA)-p(PFS/nBA)-p(DMAEMA/nBA) JNPs at pH =3 (C), pH = 4 (D), pH = 8 (E), and pH = 10 (F), respectively, and optical images of dodecane-in-water emulsion droplets (C′, D′, E′, F′) stabilized by p(MMA/nBA)-p(PFS/nBA)-p(DMAEMA/nBA) JNPs at pH 3, 4, 8, and 10, respectively.

decrease of protonation during TEM sample preparation due to evaporation of HCl.

One of the intriguing applications of tunable JB is the ability of JNPs to stabilize oil droplets in water known as Pickering emulsions. After removing excess surfactant molecules (3 days dialysis), 5 % w/w JNPs solutions were utilized to stabilize dodecane droplets in water to form Pickering emulsions. Figure 4(A−F) shows the photographs of Pickering emulsions prepared under magnetic stirring at 2000 rpm for 10 min at 25 °C which were oil-in-water determined by drop tests showing that the Pickering emulsions disperse readily in water. As shown, while p(MMA/nBA) particles are not capable of stabilizing oil droplets (Figure 4A) and p(MMA/nBA)-p(PFS/nBA) can stabilize only 15% of oil droplets (Figure 4B), the p(MMA/nBA)-p(PFS/nBA)-p(DMAEMA/nBA) JNPs are able to stabilize the Pickering emulsions for more than 2 months (Figure 4D−F), which is attributed to higher adsorption energy of amphiphilic JNPs at oil/water interface than that of spherical particles.[24] Figure 4C′−F′ show the optical images of dodecane-in-water droplets stabilized by JNPs at pH = 3, 4, 8, and 10, respectively. As seen, JNPs with smaller JB values (3.42 at pH = 10) are able to generate stable smaller oil droplets. However, as the JB value increase to 4.52 under acidic conditions (pH = 4), the oil droplets become larger (Figure 4D). And when the JB increased further at pH = 3, oil droplets become even larger (Figure 4C′) and the oil phase starts to separate from the Pickering emulsion phase. As a result, 35% of the dodecane is released in one day (Figure 4C), which is attributed to desorption of JNPs from the oil−water interface into water phase due to protonation of the pDMAEMA component. As pH decreases further to pH = 2, all oil droplets can be released in less than 1 h.

It should also be noted that insignificant droplet size changes were observed when Pickering emulsions were subjected to 30, 35, 45, and 50 °C temperatures for over 2 months. As we recall, individual JNPs exhibit significant temperature sensitivity manifested by the size and JB changes, but acidic and/or basic environments have relatively small influence on their responsiveness. In contrast, temperature changes do not significantly influence the stability of oil-in-water emulsions, whereas the residual surface charges on JNPs do, signifying that interfacial energy plays a major role on stability of Pickering emulsions.

In summary, these studies show the synthesis of triphasic stimuli-responsive JNPs that consist of phase-separated p(MMA/nBA), p(PFS/nBA), and p(DMAEMA/nBA) copolymers. These JNPs are capable of shape and size changes as a function of pH and temperature. As the temperature increases, the particle size of JNPs decreases from 147 nm at 25 °C to 131 nm at 45 °C and the particle morphology of the JNPs also changes from spherical with a convex p(PFS/nBA) phase to ellipsoidal with a concave p(PFS/nBA) phase while the JB decreased from 3.78 to 0.72. As pH decreases from 10 to 4, the particle size of JNPs increases from 145 to 163 nm while the JB increased from 3.42 to 4.52. The use of size- and JB-tunable JNPs may offer many applications ranging from stabilization of oil in water at high pH environments to environmentally compliant petroleum recovery processes, or multi-drug delivery applications in which each phase may serve as a delivery and release vehicle under desired physiological conditions.

■ EXPERIMENTAL SECTION

Preparation of stimuli-responsive JNPs: MMA, nBA, PFS, DMAEMA, and sodium dioctylsulfosuccinate (SDOSS), 2,2′-azobis(isobutyronitrile) (AIBN), 0.1 N volumetric standard solutions of sodium hydroxide (NaOH) and hydrochloride acid (HCl) were purchased from Aldrich Chemical Co. Water-soluble initiator 2,2′-azobis[2-(2-imidazolin-2-yl)propane] dihydrochloride (VA-44) was purchased from Wako Pure Chemicals Ind. Ltd. The particles shown in Figure 1 were synthesized via conventional emulsion polymerizations. (1) p(MMA/nBA) colloidal dispersion was synthesized using

dx.doi.org/10.1021/mz500029z | ACS Macro Lett. 2014, 3, 346−352

a semicontinuous process outlined elsewhere.[17] The reaction flask was immersed in a water bath preheated to 75 °C and purged continuously with N_2 gas. The reactor was first charged with 15 mL of double deionized water (H_2O), and after purging N_2 for 30 min, the content was stirred at 350 rpm. At this point, pre-emulsion (H_2O, 15 mL; SDOSS, 0.18 g, MMA, 3.0 g; nBA, 3.0 g) was fed continuously over 4 h while initiator solution (VA-044, 0.012 g; H_2O, 5 mL) was fed over 4.5 h. After completion of pre-emulsion feeding, the reaction was continued for additional 10 h. (2) Withdraw half of the p(MMA/nBA) seed emulsion, and pre-emulsion (H_2O, 15 mL; SDOSS, 0.12 g; PFS, 1.8 g; nBA, 1.8 g) was fed continuously over 4 h into the remained half p(MMA/nBA) emulsion while initiator solution (VA-044, 0.008 g; H_2O, 5 mL) was fed over 4.5 h. After completion of pre-emulsion feeding, the reaction was continued for additional 10 h. (3) Withdraw 2/3 of the S2 emulsion and 30 mL H_2O was added into the remained p(MMA/nBA)-p(PFS/nBA) emulsion, and pre-emulsion (H_2O, 15 mL; SDOSS, 0.15 g; DMAEMA 0.8 g; nBA, 0.8 g; AIBN, 0.01 g) was fed continuously over 3 h. After completion of pre-emulsion feeding, the reaction was continued for additional 10 h.

Particle size analysis was performed using a Microtrac Nanotrac particle size analyzer (model ULTRA) with an accuracy of ±1 nm. Potentiometric titrations were performed at 25 °C using Orion pH meter model 350 with a glass combination electrode (Orion 9202 BN). Autocalibration against standard buffer solutions was done before titration. Standard HCl and NaOH solution were utilized to adjust pH values of the Janus colloidal solutions.

Morphologies of the Janus particles were investigated using a JEOL TEM-2100 transmission electron microscope (TEM) operated at 200 kV, where the samples were diluted and deposited on a Formvar/carbon copper grid (EMS). In order to enhance the contrast of the TEM images of JNPs, each specimen was stained using osmium tetroxide vapors, as described in ref 29. This procedure allowed us to differentiate between p(DMAEMA/nBA) and p(MMA/nBA) phases by oxidizing tertiary amine groups in p(DMAEMA/nBA) copolymer, thus, giving higher electron densities. In a typical experiment, each specimen was exposed for four hours and the TEM images were collected. Since the gray scale obtained from TEM analysis is often highly subjective in the analysis, we also utilized image analysis using The Environment for Visualizing Images (ENVI; v. 3.5, Research Systems, Inc.).

Static contact angle measurements were conducted using a sessile drop technique and a Ramé-Hart goniometer coupled with a DROP image data analysis software. Ten μL drops were placed onto the flat surfaces coated by each copolymer film while an image of the drop was captured and the contact angle measured. Each copolymer was synthesized by surfactant-free emulsion polymerization with monomer composition and initiator ratio constant. These copolymers were precipitated, dissolved in toluene, and spin-coated on a glass slide.

Grazing-angle attenuated total reflectance Fourier transform infrared (GATR FT-IR) spectroscopy measurements were conducted on the film−substrate (F−S) interfaces using a Bio-Rad FTS-6000 FT-IR single-beam spectrometer set at 4 cm^{-1} resolution. A 2 mm Ge crystal with a 45° angle maintaining constant contact pressure between the crystal and the specimens was used. All spectra were corrected for spectral distortions by Q-ATR software using the Urban-Huang algorithm. The spectra are shown in Supporting Information, section 6, Figure S4.

Thermal analysis of the copolymers obtained from each step of emulsion polymerization was conducted using TA Instruments DSC Q-100. The calibration was carried out using indium and sapphire standards. Heating and cooling rates of 5 °C/min were used over the studied temperature range.

Computer modeling simulations were conducted using a classical (Newtonian) molecular dynamic theory combined with the COMPASS force field conditions on Material Studio software (Accelrys Inc., version 5.5). Three kinds of random copolymers p(MMA/nBA), p(PFS/nBA), and p(DMAEMA/nBA) were created. Each of them has 50 repeating units and was energy-minimized by Forcite calculations. In the phase-separation simulation, an amorphous cell was created by constructing two of each kind of energy-minimized copolymer chains under 3D periodic boundary conditions. And then this amorphous cell was allowed to do thermodynamic simulations, including NPT (constant number, pressure, and temperature) and NVT (constant number, volume, and temperature) processes to reach an energy-minimized state.

■ ASSOCIATED CONTENT

Supporting Information

Additional experimental details. This material is available free of charge via the Internet at http://pubs.acs.org.

■ AUTHOR INFORMATION

Corresponding Author

*E-mail: mareku@clemson.edu.

Notes

The authors declare no competing financial interest.

■ ACKNOWLEDGMENTS

The authors thank the National Science Foundation (CMMI 332964) for supporting these studies. The J. E. Sirrine Foundation as well as Electron Microscopy Laboratory at Clemson University are also ackowleged for partial support of these studies.

■ REFERENCES

(1) Roh, K. H.; Martin, D. C.; Lahann, J. *Nat. Mater.* **2005**, *4* (10), 759−763.
(2) Walther, A.; Müller, A. H. E. *Chem. Rev.* **2013**, *113* (7), 5194−5261.
(3) Du, J.; O'Reilly, R. K. *Chem. Soc. Rev.* **2011**, *40* (5), 2402−2416.
(4) Hu, J.; Zhou, S.; Sun, Y.; Fang, X.; Wu, L. *Chem. Soc. Rev.* **2012**, *41* (11), 4356−4378.
(5) Nie, Z.; Li, W.; Seo, M.; Xu, S.; Kumacheva, E. *J. Am. Chem. Soc.* **2006**, *128* (29), 9408−9412.
(6) Nisisako, T.; Torii, T.; Takahashi, T.; Takizawa, Y. *Adv. Mater.* **2006**, *18* (9), 1152−1156.
(7) Erhardt, R.; Böker, A.; Zettl, H.; Kaya, H.; Pyckhout-Hintzen, W.; Krausch, G.; Abetz, V.; Müller, A. H. *Macromolecules* **2001**, *34* (4), 1069−1075.
(8) Glotzer, S. C.; Solomon, M. J. *Nat. Mater.* **2007**, *6* (8), 557−562.
(9) Walther, A.; Mueller, A. H. E. *Soft Matter* **2008**, *4* (4), 663−668.
(10) Hong, L.; Jiang, S.; Granick, S. *Langmuir* **2006**, *22* (23), 9495−9499.
(11) Gu, H. W.; Yang, Z. M.; Gao, J. H.; Chang, C. K.; Xu, B. *J. Am. Chem. Soc.* **2005**, *127* (1), 34−35.
(12) Lu, Y.; Xiong, H.; Jiang, X.; Xia, Y.; Prentiss, M.; Whitesides, G. M. *J. Am. Chem. Soc.* **2003**, *125* (42), 12724−12725.
(13) Nie, L.; Liu, S. Y.; Shen, W. M.; Chen, D. Y.; Jiang, M. *Angew. Chem., Int. Ed.* **2007**, *46* (33), 6321−6324.
(14) Gu, H.; Zheng, R.; Zhang, X.; Xu, B. *J. Am. Chem. Soc.* **2004**, *126* (18), 5664−5665.
(15) Reculusa, S.; Poncet-Legrand, C.; Perro, A.; Duguet, E.; Bourgeat-Lami, E.; Mingotaud, C.; Ravaine, S. *Chem. Mater.* **2005**, *17* (13), 3338−3344.
(16) Zhao, N.; Gao, M. *Adv. Mater.* **2009**, *21* (2), 184−187.
(17) Misra, A.; Urban, M. W. *Macromol. Rapid Commun.* **2010**, *31* (2), 119−127.
(18) Corten, C. C.; Urban, M. W. *Polym. Chem.* **2011**, *2* (1), 244−250.
(19) Ramachandran, D.; Corten, C. C.; Urban, M. W. *RSC Adv.* **2013**, *3* (24), 9357−9364.
(20) Berger, S.; Synytska, A.; Ionov, L.; Eichhorn, K.-J.; Stamm, M. *Macromolecules* **2008**, *41* (24), 9669−9676.
(21) Tanaka, T.; Okayama, M.; Minami, H.; Okubo, M. *Langmuir* **2010**, *26* (14), 11732−11736.

(22) Jiang, S.; Chen, Q.; Tripathy, M.; Luijten, E.; Schweizer, K. S.; Granick, S. *Adv. Mater.* **2010**, *22* (10), 1060−1071.
(23) Chen, Q.; Whitmer, J. K.; Jiang, S.; Bae, S. C.; Luijten, E.; Granick, S. *Science* **2011**, *331* (6014), 199−202.
(24) Binks, B. P.; Fletcher, P. D. I. *Langmuir* **2001**, *17* (16), 4708−4710.
(25) Jiang, S.; Granick, S. *Langmuir* **2008**, *24* (6), 2438−2445.
(26) Chen, Q.; Bae, S. C.; Granick, S. *Nature* **2011**, *469* (7330), 381−384.
(27) Ho, C.-C.; Chen, W.-S.; Shie, T.-Y.; Lin, J.-N.; Kuo, C. *Langmuir* **2008**, *24* (11), 5663−5666.
(28) Ling, X. Y.; Phang, I. Y.; Acikgoz, C.; Yilmaz, M. D.; Hempenius, M. A.; Vancso, G. J.; Huskens, J. *Angew. Chem., Int. Ed.* **2009**, *48* (41), 7677−7682.
(29) Gröschel, A. H.; Walther, A.; Löbling, T. I.; Schmelz, J.; Hanisch, A.; Schmalz, H.; Müller, A. H. *J. Am. Chem. Soc.* **2012**, *134* (33), 13850−13860.
(30) Liu, F.; Urban, M. W. *Macromolecules* **2008**, *41* (17), 6531−6539.